HHS Public Access

Author manuscript

Adv Mater. Author manuscript; available in PMC 2016 February 11.

Published in final edited form as:

Adv Mater. 2015 February 11; 27(6): 1083–1089. doi:10.1002/adma.201404849.

Flexible and stretchable micromagnet arrays for tunable biointerfacing

Dr. Peter Tseng, **Jonathan Lin**, **Keegan Owsley**, **Janay Kong**, **Dr. Anja Kunze**, **Coleman Murray**, and **Prof. Dino Di Carlo**

Department of Bioengineering, 420 Westwood Plaza, 5121E Engineering V, Los Angeles, CA, 90095

Dino Di Carlo: dicarlo@ucla.edu

Abstract

We develop a process to surface pattern PDMS with ferromagnetic structures of varying sizes (micron to mm) and thicknesses (> 70 micron). We utilize their flexibility and magnetic reach to confer dynamic, additive properties to a variety of substrates such as coverslips and eppendorf tubes. We find these substrates can generate additional modes of magnetic droplet manipulation, and can tunably steer magnetic-cell organization.

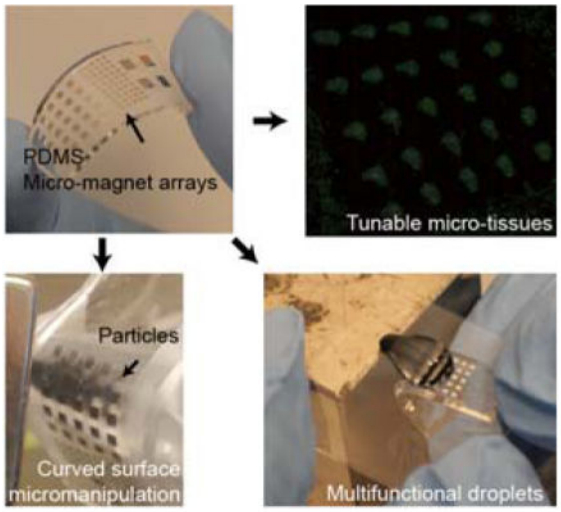

Keywords

Flexible electromagnetics; magnetic separation; magnetic droplet; biomagnetism; bioseparation

Devices integrated onto deformable substrata[1,2] have tremendous potential in bringing unique technical capabilities to a wide variety of environments, such as within the body

Correspondence to: Dino Di Carlo, dicarlo@ucla.edu.

Supporting Information

Supporting Information is available from the Wiley Online Library or from the author.

(with epidermal and transient electronics[3,4]), on curved surfaces (such as monitors, solar cells, and displays[5–7]), and in biotechnology[8,9]. Flexible magnetic devices, in particular, have unique potential as an approach by which researchers could dynamically and remotely interface with biomatter. Such devices could provide a shape-conforming and reconfigurable alternative to more complex micromanipulation approaches, which typically involve direct micromachining of microchips via microcoils[10,11] or patterned ferromagnetic material[12–15]. The majority of current flexible magnetic devices comprise of micron-scale, physically-addressable magneto-structures (e.g. magnetic cilia), not typically produced with wafer-scale processes[16–20]. Magnetic-electronic devices integrated on plastic substrates have similarly been studied to lend sensing capabilities to more diverse environments[21–23].

In this paper, we develop a new manufacturing method to surface micromachine electroplated magnetic materials (of diverse size) on elastomeric materials, and use these hybrid, flexible magnetic materials to confer additive properties to common substrates in biotechnology, such as eppendorf tubes, coverslips, fluidic channels. Structures are fabricated via direct micromachining on thin films with tunable solubility (rendered only soluble in water with monovalent ions, such as salt) to micromachine robust films of permalloy, which are subsequently sacrificed and surface patterned on PDMS of varying elastic moduli (below 100 kPa). We demonstrate the ability to generate a broad range of sizes (4 μm to centimeter scales width and length, with thicknesses of >70 μm), and reliable transfer of near wafer-scale micromachined chips onto PDMS (over a 5 cm length scale). The versatility of this approach allows us to generate designed, micro-machined magnetic structures that convey precision and broad interfacing with commonly used biological substrata such as conical tubes, coverslips, and fluidic channels. We find that by exploiting their inherent adhesive and elastic properties, these films can enhance magnetic separation in microfluidic channels, achieve magnetic particle patterning and micromanipulation on curved surfaces, confer additional capabilities during magnetic droplet manipulation, and magnetically pattern biomatter[24,25] via spatial morphing of the ultrasoft magnetic-PDMS chips.

Metal structures are commonly patterned onto PDMS via contact printing techniques, or water-soluble transfer layers[26–29]. Formation of ferromagnetic metals on PDMS, however, is challenging due to poor adhesion of these materials to PDMS. Commonly used approaches utilize electrolyte stamping followed by electroless plating[30], or exploit the poor adhesion strength of metals and oxides to thin films of gold[20,31]. While these approaches are stable for thin (< 1 μm thick) or physically small structures (and thus possessing low stress), large and thick films of electroplated ferromagnetic material, needed for strong force generation and actuation, have not been demonstrated using these previous approaches. This is presumably due to large intrinsic stresses that develop during and after metal deposition[32]. Also unclear is the compatibility of such approaches to functionalizing silicones of much lower elastic moduli (~100 kPa).

To overcome these potential issues, we fabricated magnetic-PDMS hybrid materials using an approach similar to techniques we used to directly micro-machine above dextran thin films[33]. Due to the electroplating process required for thick film ferromagnet deposition (which occurs in an acidic plating bath), dextran films can become unstable during

deposition. Because of this, we adapted previously characterized poly-acrylic acid[34] thin films for the micromachining of our ferromagnetic material (Suppl. Fig. 1). Poly-acrylic acid films can be rendered insoluble in water via soaking in $CaCl_2$, which crosslinks the network to form insoluble Ca^{2+}-PAA. This film is stable in the presence of high concentrations of bivalent ions, which can include Ni^{2+} and Fe^{2+}, in addition to Ca^{2+}. This film can subsequently reacquire water solubility via the introduction of monovalent ions, such as Na^{+}. After Ca^{2+}-PAA layer deposition, we treated the surface with air plasma and evaporated a seed layer of Ti-Cu-Ti to form the base of the electroplated magnetic material. Micro-magnets can generally be patterned using either positive or negative photoresists. Due to the high stresses developed during negative photoresist stripping (which rely on swelling and subsequent delamination of the resin), we saw mixed results using these resists that were dependent on factors such as the Ca^{2+}-PAA treatment, permalloy thickness, resin thickness, and resin development cycle. Due to these reasons, for features generated in the manuscript we used exclusively positive photoresists, which can be etched directly with acetone. This, however, places a limit on the thickness of our generated structures to around 100 μm. Ultimately, negative resist optimization would need to be done to generate thicknesses on the millimeter height scale with SU-8. To ensure proper bonding to PDMS, we sputtered a thin layer of titanium (30 nm), and silanized this layer to yield allyl functionality[35] for direct cross-linking with PDMS. This direct bonding of metals to PDMS avoids silicon dioxide intermediate layers, which are highly brittle and crack under minimal strain. Ca^{2+}-PAA layers were typically etched in NaCl-water over 24 hours on a shaker. Larger chips (> 2.5 cm) can take longer to sacrifice, and we typically expedited this process using gentle plying of the PDMS with tweezers.

We integrated magnetic elements into a variety of PDMS films comprised of varying properties, including 1) thick, stiff layers, 2) thin membranes, and 3) thick, ultra-flexible layers of PDMS (Figure 1, Supp. Fig. 1). These flexible materials handle differentially, and manipulate uniquely under magnetic field stimuli (Supp. Fig. 2). Due to the large size and volume of deposited material, our chips could be manipulated readily nearby a magnet. In general, we used thick, stiffer PDMS structures to interface with flat substrates such as slides, thinner membranes of PDMS for wrapping around eppendorf tubes, and ultra-flexible layers for experiments that require complex warping of the magnetic structures. Magnetic-PDMS with moduli ~100 kPa were highly stable under stretch approaching 200 % and more of initial size. Structures did not crack, and retained their initial positions upon relaxation under these conditions (Figure 1c).

We simulated the magnetic fields generated by our micromagnets at the length scales of coverslips and eppendorf tubes using COMSOL finite-element-modeling (Supp. Fig. 3). We found incident fields of around B_n = 20 mT and B_t = 8.7 mT to be enough to manipulate magnetic particles within droplets (magnetic field shown in Supp. Fig. 3c, corresponding to magnetic field gradients of 2 A/m^2 and lower at a coverslips distance from the micromagnet array). The cross-section of local magnetic fields generated by individual micromagnets when placed adjacent to a permanent magnet is given in Supp. Figure 3d. To study inaccuracies in our model, we directly measured the velocity of manipulated Spherotech particles (4.4 μm, B_{sat}=.045 T, in water) via a high-speed camera with a magnet placed at

approximately 1 cm (and askew) from the magnetic elements. At a coverslips' distance away from our micro-magnet array, particles moved at velocities close to 1 mm/s. Using Stokes' law for viscous drag (and using the viscosity of water), this corresponds to forces of close to 30 pN on single particles, and a field gradient of up to 16 A/m^2 (Figure 2, Suppl. Video 1), before becoming trapped close to the magnet. Simulated field gradients place magnetic force at slightly lower values, of around 18 pN (Supp. Fig. 3a). The inaccuracies are likely due to 1) difficulties in controlling the distance of the magnet from the substrate (incident field fluctuates with position), 2) simulation of a single magnet rather than an array, and 3) difficulty in verifying single particles manipulating in the field. In general, simulations accurately predict the trapping position of particles, and forces at saturating input magnetic fields[13]. Because magnetic forces scale by volume of the manipulated magnetic material, the time scale at which particles organize would increase from smaller sized particles. For example, the Spherotech particles used for many of our experiments organize within less than a second. However, particles an order of magnitude smaller, possessing hydrodynamic diameters of 440 nm would require almost 3 orders of magnitude longer to organize, taking up to 5 to 10 minutes (indeed, manipulation of 250 nm particles required these timescales). In general, for substrate thicknesses of 100 μm to 250 μm, particles of 2 μm (Bsat~.05 T) and larger are required for efficient (sub 1 minute) manipulation within fluidic droplets on hydrophobic surfaces (30 μL). This becomes less critical when the height of the particle solution becomes limited, such as within microfluidic channels or on hydrophilic surfaces.

We utilized this trapping effect to contour the flow path of magnetic particles in microfluidic channels by morphing soft magnetic-PDMS elements flanking the bottom of coverslip-mounted microfluidic channels (Figure 2c, Suppl. Video 2). We trapped particles around micromagnetic elements, and subsequently released these to lower incident fields. Released particles flowed along pathways delineated by the reconfigurable morphed micromagnet array. This dynamically tunable microfluidic magnetophoresis compares well to more traditional microchannel particle manipulation techniques such as dielectrophoresis[36]. Dielectrophoretic approaches, due to lower inherent forces generated compared to labelled magnetic approaches (permeability differences far exceed permittivity differences), typically require micropatterned conductive electrodes directly adjacent to the microchannel to mediate particle manipulation. Also due to lower forces, magnetophoretic approaches typically possess larger manipulation ranges, and high-throughput than dielectrophoretic counterparts. Focusing positions of dielectrophoretic manipulated particles, however, are highly repeatable compared to magnetophoretic approaches[37].

We tested the capability of arrays of micromachined structures to pattern magnetic structures within flat and along curved surfaces (Figure 3) using magnetic matrices of 500 μm or 1 mm squares. We were able to pattern magnetic particles (Spherotech, 4.4 μm) within eppendorf tubes, and within fluidic droplets under relatively low incident magnetic fields (20 mT). These particles could be readily micromanipulated within these structures by reorienting the magnetic elements in relation to the permanent magnet. The characteristic manipulation behavior of magnetic particles under a rotating field is shown in Figure 3b, and displays a phase lag as a result of hysteresis in the ferromagnetic structure.

We subsequently utilized the flexible properties of our substrates to confer tunable, additive capabilities to magnetic droplet manipulation. Firstly, the addition of the flexible micromagnet array protects the arrayed particles against large scale manipulation of the main permanent magnet, allowing selective manipulation of magnetic droplets. Secondly, by selectively removing particles from their associated local micro-magnet, particles were then free to either be extracted from the droplet, or to manipulate the droplet itself (Figure 3d and e). This allows the generation of two additional droplet behaviors: 1) sub-selection of particles for controlled extraction, and 2) formation of bipolar magnetic droplets, possessing both leading and retracting edges of magnetic particles within a single droplet. We were unable to manipulate droplets directly with our designed micromagnet sizes (up to 3 × 3 mm) due to inability to generate the required aggregate forces. We suspect that patterning larger magnetic structures (> 1 cm) could generate these forces and facilitate direct droplet manipulation/extraction. Extraction of specific subpopulations of particles from droplets could potentially allow for sequential time-dependent analysis of chemical environments within a droplet (e.g. cytokine production from captured immune cells).

We finally examined how ultra-soft layers of magnetic-PDMS could form a dynamic yet simple, reusable interface to pattern biological structures on standard coverslips used in biological labs. We generated magnetizable cells by dosing HeLa cells with magnetic nanoparticles, and subsequently seeded these onto a single coverslip flanked by two magnetic matrices of 500 μm elements integrated into soft PDMS (40:1). One matrix we left in a native conformation, while the second we morphed in both x- and y-dimensions to form a strained structure (Figure 4a). The low elasticity of the PDMS allowed the morphed structure to remain structurally stable purely due to non-covalent stiction of the PDMS to the glass coverslip. Upon application of a permanent magnet, cells manipulated into cell aggregates, shaped by the local magnetic field generated by the micro-magnets (Supp. Fig. 4). More interestingly, several hours after adhering, these aggregates exhibit characteristics similar to tissues patterned via surface patterning, such as larger internal populations of cells and the parallel elongation of cells along the structure edge. We also found that tuning the orientation of the magnet with the external field yielded uniquely polarized 2-d biostructures (Supp. Fig 5). These cell patterns possessed some 3-d characteristics, as large, local fields force cells to grow above each other. The size of these individual structures correlated well with respective cell counts (Figure 4b), and biostructures at the edge of the magnetic matrix generally had higher cell counts in comparison to those in the interior. A comparison of the orientation of generated cell patterns in unstrained versus morphed matrices demonstrated the spread of pattern orientation as a result of the morphed micromagnet array. Cell patterns oriented broadly over 80 degrees over morphed patterns, in comparison to 10 degree spread over unstrained features. Cell patterns formed by morphed structures also possessed unique shapes as a result of complex angular interactions between the incident field and the micromagnets (Supp. Fig 4).

In total, we demonstrate a versatile method of integrating high quality permalloy features of varying size (4 μm to 5 mm) and thickness (1 μm to 70 μm) into PDMS of varying elastic properties (10:1 to 50:1) using poly-acrylic acid thin films. We utilize the versatility of this process to generate various unique, additive behaviors in commonly used substrates in a biology laboratory. We found that different forms of magnetic-PDMS co-structures could

integrate seamlessly alongside coverslips, eppendorf tubes, and fluidic channels to micro-manipulate particles and form biostructures; this may potentially generate new applications in magnetic droplet control, magnetophoresis, bio-patterning, and self-assembly. The simplicity and usability of these structures compare favorably to the complexity of the dynamic, tunable particle manipulation demonstrated by optical approaches (specifically optoelectronic traps). While OET systems possess superior tunability and scalability, these systems require a photoconductive and transparent interfacial layer (such as indium tin oxide) and an underlying electrode[38,39], thus being difficult to operate on non-traditional substrates such as curved surfaces. These material requirements also prohibit the ability to "tag" their capabilities onto other substrates. Our demonstrated flexible micromagnetic structures could potentially integrate alongside biological structures such as the epidermis or blood vessels, and—for example—be utilized alongside antigen-scavenging magnetic particles[40] to trap and micro-manipulate biological matter directly within biofluids.

Experimental

Substrate preparation

Details for substrate fabrication can be found our Supporting Information.

Microfluidics

A 375 μm-thick, 1.2 mm-wide channel was fabricated using SU-8 2100 photolithography and subsequent soft lithography, and bonded to a #1.5 coverslip. An array of magnets was morphed and flanked against the surface. For routing experiments, magnetic particles (Spherotech, 4.4 μm, Nile Red fluorescent) were flowed in the channel, and initially captured against a 50 μl/min flow by application of a magnet above the channel (and askew from the light source). The flow rate (switched to water) was subsequently increased to 100 μl/min and the magnet was slowly removed to reduce the capture field gradient.

Magnetic droplet micropatterning

We used carboxyl-ferromagnetic particles (Spherotech, 4.4 μm, B_{sat}=.045 T) to demonstrate magnetic patterning and magnetic droplet manipulation. We used two NdFeB magnets for experiments: a cube (1 in, N52, K&J Magnetics), or a cylinder (1 ¾ in x ¼ in, N42). Flexible magnetic structures (500 μm-wide) were attached directly to our desired substrate, and subsequently oriented around a permanent magnet to acheive desired functionality. For curved substrate patterning, membranes or sheets of magnetic-PDMS were wrapped conformally around the eppendorf tube. Magnetic particles were patterned within the tube from a 1:10 dilution of particles in water. For micro-manipulation of particles, a 50 μL droplet of magnetic particles was applied to a coverslip flanked by magnetic-PDMS, and this structure was then rotated around our cylindrical magnet. Droplet manipulations occured on teflon-coated coverslips. 1 % Teflon AF (Sigma) was dissolved in Fluorinert FC-40 (Sigma), spun on coverslips, and annealed for 30 seconds at 300 degrees. 50 μL droplets were applied above magnetic-PDMS tagged coverslips, and initially patterned at a distance of 1.5 inches from our cubic permanent magnet. These coverslips could then be oriented close to the permanent magnet and patterned magnetic particles could be selectively untagged by flexing of the PDMS substrate. Untagged particles were then manipulated by

the permanent magnet to acheive the two base magnetic particle actuation regimes: particle extraction and droplet actuation.

2-d microtissue formation

A 2-mm thick PDMS stencil was placed above a coverslip to form a cell-culture well. Two magnetic arrays of 500 μm elements integrated onto 40:1 PDMS were applied to the coverslip, one unstrained, and one strained. Magnetic nanoparticle-dosed HeLa cells were pipetted into the PDMS well, and the combined substrate was oriented slowly onto our cylindrical magnet (moved from 2 inches to directly above the magnet over a 5 minute timepan). This was then cultured in an incubator over 8 hours. Samples were then fixed and stained for analysis, as in previous studies[33,35].

Supplementary Material

Refer to Web version on PubMed Central for supplementary material.

Acknowledgments

This work was partially supported through the NIH Director's New Innovator grant (1DP2OD007113). We thank Jerry Wu for fabrication of the microfluidic mold, and the UCLA Nanoelectronics Research Facility. Anja Kunze thanks the Swiss National Science Foundation (SNSF) for supporting this project under the grant P300P2_147753. Jonathan Lin acknowledges the NIH MSTP Training Grant # T32GM008042.

References

1. Khang DY, Jiang H, Huang Y, Rogers JA. Science. 2006; 311:208. [PubMed: 16357225]
2. Kim DH, Rogers JA. Adv Mater. 2008; 20:4887.
3. Kim DH, Lu N, Ma R, Kim YS, Kim RH, Wang S, Wu J, Won SM, Tao H, Islam A, Yu KJ, Kim T, Chowdhury R, Ying M, Xu L, Li M, Chung HJ, Keum H, McCormick M, Liu P, Zhang YW, Omenetto FG, Huang Y, Coleman T, Rogers JA. Science. 2011; 333:838. [PubMed: 21836009]
4. Hwang SW, Tao H, Kim DH, Cheng H, Song JK, Rill E, Brenckle MA, Panilaitis B, Won SM, Kim YS, Song YM, Yu KJ, Ameen A, Li R, Su Y, Yang M, Kaplan DL, Zakin MR, Slepian MJ, Huang Y, Omenetto FG, Rogers JA. Science. 2012; 337:1640. [PubMed: 23019646]
5. Lipomi DJ, Tee BCK, Vosgueritchian M, Bao Z. Adv Mater. 2011; 23:1771. [PubMed: 21491510]
6. Sekitani T, Nakajima H, Maeda H, Fukushima T, Aida T, Hata K, Someya T. Nat Mater. 2009; 8:494. [PubMed: 19430465]
7. Ju S, Facchetti A, Xuan Y, Liu J, Ishikawa F, Ye P, Zhou C, Marks TJ, Janes DB. Nat Nanotechnol. 2007; 2:378. [PubMed: 18654311]
8. Zheng Y, He Z, Gao Y, Liu J. Sci Rep. 2013; 310.1038/srep01786
9. Ko H, Lee J, Kim Y, Lee B, Jung CH, Choi JH, Kwon OS, Shin K. Adv Mater. 2014; 26:2335. [PubMed: 24729060]
10. Ramadan Q, Yu C, Samper V, Poenar DP. Appl Phys Lett. 2006; 88:032501.
11. Lee H, Purdon A, Westervelt R. Appl Phys Lett. 2004; 85:1063.
12. Tseng P, Di Carlo D, Judy JW. Nano Lett. 2009; 9:3053. [PubMed: 19572731]
13. Tseng P, Judy JW, Di Carlo D. Nat Methods. 2012; 9:1113. [PubMed: 23064517]
14. Zanini LF, Dempsey NM, Givord D, Reyne G, Dumas-Bouchiat F. Appl Phys Lett. 2011; 99:232504.
15. Derec C, Wilhelm C, Servais J, Bacri JC. Microfluid Nanofluidics. 2010; 8:123.
16. Kim J, Chung SE, Choi SE, Lee H, Kim J, Kwon S. Nat Mater. 2011; 10:747. [PubMed: 21822261]

17. Shields AR, Fiser BL, Evans BA, Falvo MR, Washburn S, Superfine R. Proc Natl Acad Sci. 2010; 107:15670. [PubMed: 20798342]
18. Sniadecki NJ, Anguelouch A, Yang MT, Lamb CM, Liu Z, Kirschner SB, Liu Y, Reich DH, Chen CS. Proc Natl Acad Sci. 2007; 104:14553. [PubMed: 17804810]
19. Timonen JVI, Johans C, Kontturi K, Walther A, Ikkala O, Ras RHA. ACS Appl Mater Interfaces. 2010; 2:2226. [PubMed: 20695442]
20. Zhu Y, Antao DS, Xiao R, Wang EN. Adv Mater. 2014 n/a.
21. Chen Y, Mei Y, Kaltofen R, Mönch JI, Schumann J, Freudenberger J, Klauβ HJ, Schmidt OG. Adv Mater. 2008; 20:3224.
22. Melzer M, Karnaushenko D, Makarov D, Baraban L, Calvimontes A, Mönch I, Kaltofen R, Mei Y, Schmidt OG. RSC Adv. 2012; 2:2284.
23. Karnaushenko D, Makarov D, Yan C, Streubel R, Schmidt OG. Adv Mater. 2012; 24:4518. [PubMed: 22761017]
24. Souza GR, Molina JR, Raphael RM, Ozawa MG, Stark DJ, Levin CS, Bronk LF, Ananta JS, Mandelin J, Georgescu MM, Bankson JA, Gelovani JG, Killian TC, Arap W, Pasqualini R. Nat Nanotechnol. 2010; 5:291. [PubMed: 20228788]
25. Okochi M, Takano S, Isaji Y, Senga T, Hamaguchi M, Honda H. Lab Chip. 2009; 9:3378. [PubMed: 19904404]
26. Carlson A, Bowen AM, Huang Y, Nuzzo RG, Rogers JA. Adv Mater Deerfield Beach Fla. 2012; 24:5284.
27. Karlsson JM, Haraldsson T, Carlborg CF, Hansson J, Russom A, van der Wijngaart W. J Micromechanics Microengineering. 2012; 22:085009.
28. Lim KS, Chang WJ, Koo YM, Bashir R. Lab Chip. 2006; 6:578. [PubMed: 16572223]
29. Meitl MA, Zhu ZT, Kumar V, Lee KJ, Feng X, Huang YY, Adesida I, Nuzzo RG, Rogers JA. Nat Mater. 2006; 5:33.
30. Koschwanez JH, Carlson RH, Meldrum DR. Rev Sci Instrum. 2007; 78:044301. [PubMed: 17477681]
31. Donolato M, Tollan C, Porro JM, Berger A, Vavassori P. Adv Mater. 2013; 25:623. [PubMed: 23108927]
32. Glickman M, Tseng P, Harrison J, Niblock T, Goldberg IB, Judy JW. J Microelectromechanical Syst. 2011; 20:842.
33. Tseng P, Pushkarsky I, Di Carlo D. PLoS ONE. 2014; 9:e106091. [PubMed: 25153326]
34. Linder V, Gates BD, Ryan D, Parviz BA, Whitesides GM. Small Weinh Bergstr Ger. 2005; 1:730.
35. Tseng P, Di Carlo D. Adv Mater. 2014; 26:1242. [PubMed: 24323894]
36. Cetin B, Li D. Electrophoresis. 2011; 32:2410. [PubMed: 21922491]
37. James CD, McClain J, Pohl KR, Reuel N, Achyuthan KE, Bourdon CJ, Rahimian K, Galambos PC, Ludwig G, Derzon MS. J Micromechanics Microengineering. 2010; 20:045015.
38. Chiou PY, Ohta AT, Wu MC. Nature. 2005; 436:370. [PubMed: 16034413]
39. Wu MC. Nat Photonics. 2011; 5:322.
40. Kang JH, Super M, Yung CW, Cooper RM, Domansky K, Graveline AR, Mammoto T, Berthet JB, Tobin H, Cartwright MJ, Watters AL, Rottman M, Waterhouse A, Mammoto A, Gamini N, Rodas MJ, Kole A, Jiang A, Valentin TM, Diaz A, Takahashi K, Ingber DE. Nat Med. 2014; 20:1211. [PubMed: 25216635]

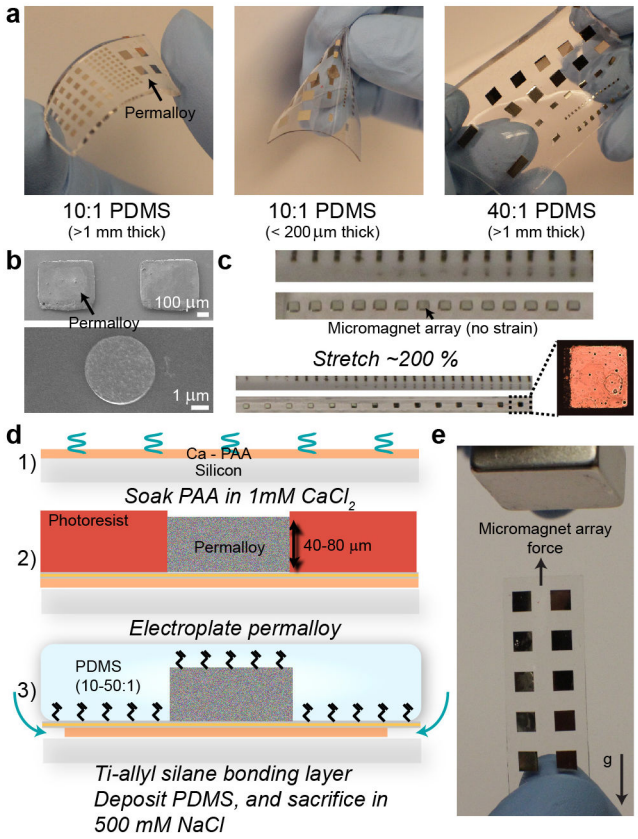

Figure 1.

Integration of varying thicknesses and sizes of permalloy structures into PDMS of varying elastic properties. a) Deflection properties of varying “flavours” of ferromagnet-embedded PDMS (with different thicknesses and elasticities). Thin PDMS membranes can be folded, while metal structures on 40:1 PDMS can be morphed in x- and y-dimensions. b) SEM images of 500 μm and 4 μm permalloy features after titanium sputtering. c) Stretch behavior of elements bonded to 40:1 PDMS. Permalloy elements retain initial size, and remain crack-free despite significant deformation of the PDMS. Each tick is 1 mm. d) Abbreviated process flow. A more detailed process flow is given in the Supporting Information. e) Matrix of 3 mm permalloy elements on a PDMS membrane directly manipulated by a permanent magnet. Under no force, the membrane folds down due to gravity, but due to forces generated by the permanent magnet remains upright.

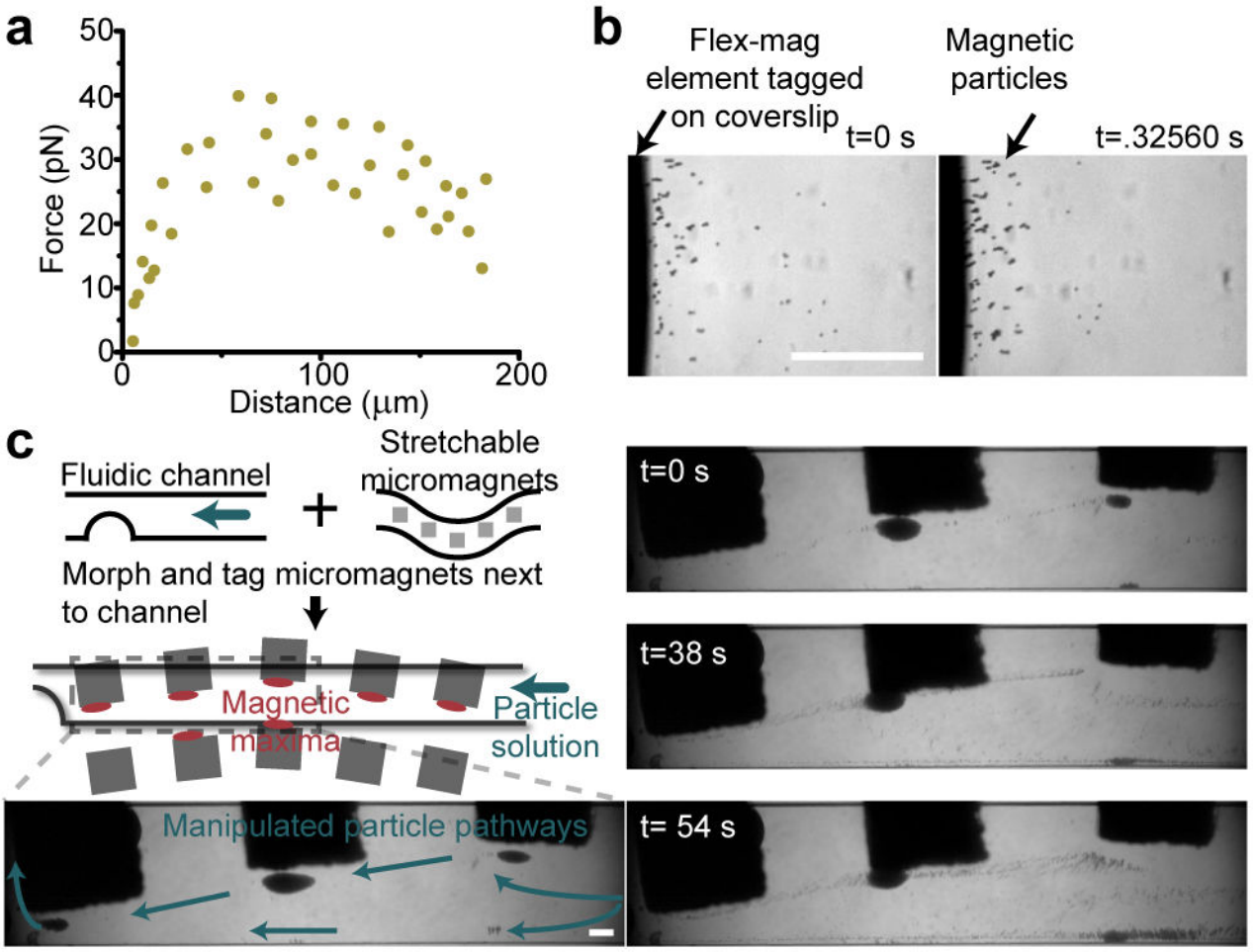

Figure 2.

Characterization of magnetic forces in fluidic flow. a) Extracted force as a function of position from two particle traces. This is at a coverslips' distance away from the micromagnet array. b) Images of localized magnetic particles at two time points of high-speed capture of particles at a tagged-coverslip surface. Particles rapidly aggregate at magnetic field minima. c) Diagram of the additive potential of our stretchable micromagnet array. A simple microfluidic channel is tagged by our magnetic material. Selected frames are from a time-lapse movie of particles manipulated against fluidic flow. Blue arrows indicate direction of particle manipulation against the driving fluid. Particles can be tunably manipulated against the fluidic flow of the channel via positional morphing and tagging of the flexible micromagnet array. Scale bars are 200 μm.

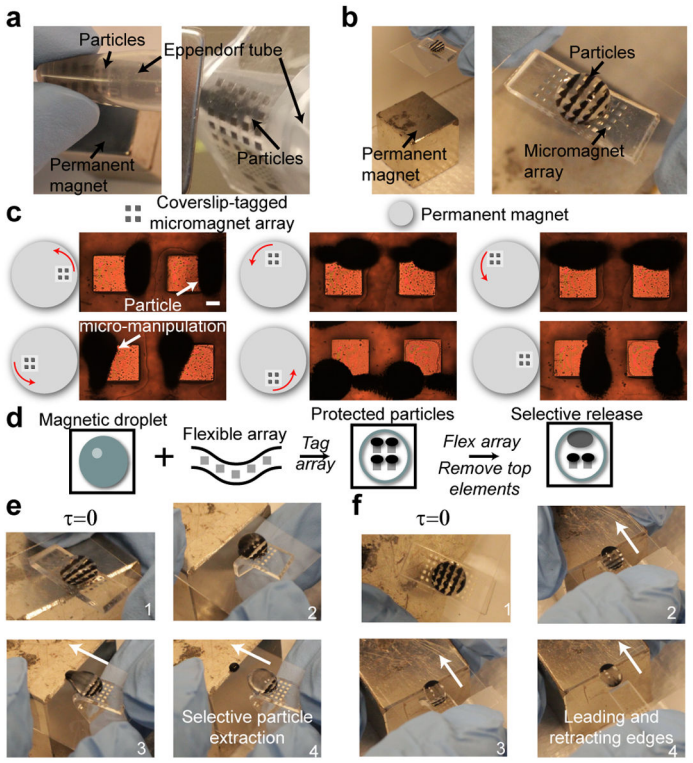

Figure 3.

Additive micropatterning of magnetic particles. a) Particles micro-manipulated on curved surfaces (an eppindorf tube) wrapped by a PDMS membrane (left) and thick film (right). b) Particles can be manipulated at relatively large distances from the permanent magnet, and form repeatable particle networks. c) Controlled micro-manipulation of magnetic particles on coverslips above micromagnets under a rotating magnetic field. d) Diagram of dynamic and tunable interactivity of magnetic droplets with our taggable micromagnet array. The micromagnet array prevents particles from being manipulated by permanent magnet. Deprotecting particles by flexing the underlying array releases the particles for subsequent manipulation. e) Selective particle extraction via manipulation of the underlying magnetic matrix, allowing temporal subselection of magnetic particles from a single droplet. e) Formation of unique, bipolar magnetic droplets, which possess leading and retracting particle edges during magnetic droplet manipulation above micro-magnet matrix. Scale bar is 200 μm.

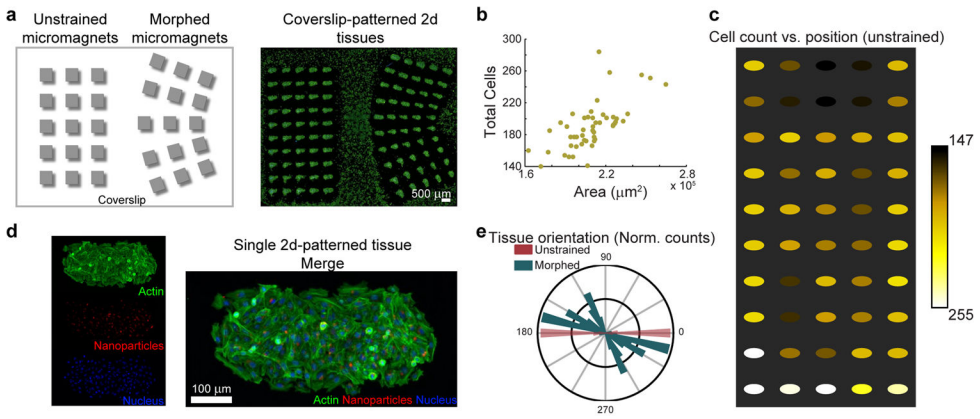

Figure 4.

Tunable cancer spheroid patterning. a) Magnetic particle-dosed cells patterned onto unstrained, and morphed flexible micro-magnet arrays on PDMS (40:1). b) Plot of the total cells as a function of the micro-tissue area. There is a strong correlation between the patterned tissue area and their respective cell count. c) Cell count as a function of tissue position. Micro-magnets at the matrix edges generally localize more cells than in the interior. d) Fluorescent microscopy of a single 2-d spheroid. e) Normalized histogram of micro-tissue orientation in unstrained and morphed structures. Morphed micro-magnets generated a large spread in orientation angle (and in micro-tissue shape) due to the complex interaction between the morphed micro-magnets and the external magnetic field.